Mechanism and Machine Theory 116 (2017) 248–261

Contents lists available at ScienceDirect

Mechanism and Machine Theory

journal homepage: www.elsevier.com/locate/mechmachtheory

Research paper

Design of variable impedance actuator for knee joint of a portable human gait rehabilitation exoskeleton

Rafael R. Torrealba*, Samuel B. Udelman, Edgar D. Fonseca-Rojas

Biomechanics and Mechatronics Research Groups, Simón Bolívar University, Caracas 1080A, Venezuela

ARTICLE INFO

Article history:
Received 18 January 2017
Revised 2 May 2017
Accepted 31 May 2017
Available online 12 June 2017

Keywords:
Variable impedance actuator
Variable stiffness mechanism
Human knee joint
Gait rehabilitation exoskeleton
Robotic-assisted gait training

ABSTRACT

This paper presents the design of a variable impedance actuator, called BAFSA, for the knee joint of a portable human gait rehabilitation exoskeleton. Such an actuator is specifically tailored to this joint, aimed at the application of robotic-assisted gait training therapies to restore the normal function of the impaired knee, taking into account kinematics, kinetics and anthropometric requirements along the gait cycle. Mechanical design and functioning of the actuator are thoroughly shown, with particular emphasis upon the variable stiffness mechanism, which consists of an axial floating spring, bidirectionally actuated in an antagonistic way. This is combined with a complimentary system, named BLAPS, that allows to vary automatically the preload stiffness, and sustain it before external loads with no further energy cost to the actuator motors. Simulations reproducing a normal gait cycle on level terrain are carried out to demonstrate the feasibility of the design, considering both power and energy consumption to validate the actuator performance. Thus, the actuator here developed is suitable to implement different rehabilitation strategies on the impaired knee joint. Finally, complete disclosure is achieved by presenting the technical specifications of the BAFSA, which fulfills all the requirements that were initially established as design criteria.

1. Introduction

Robotic advancements applied to wearable devices have enhanced rehabilitative possibilities in humans. Rehabilitation exoskeletons are the pinnacle of such biomechatronic systems, which may restore the lower limb motion of physically impaired persons [1–3]. In particular, patients with spinal cord injuries or after stroke usually need gait rehabilitation for relearning the basic functions of gait [4–7]. This requires intensive and task-specific training suitable to be applied via a robotic device, such as an exoskeleton. The idea is to evolve from repetitive slow motion of the legs to a more fluent sequence of gait phases, toward an increasing participation of the patient until full, or at least, reasonable recovery of the mobility functions [8–10]. For this, it is important to modulate the level of force exerted on the legs, either for making movements or assisting movements during gait, in accordance to the specific level of impairment presented by the patient treated along a given therapy. Hence, such a rehabilitation process via a robotic device must involve modulation of the compliance of the joint actuators to impose, assist-as-needed, or follow a human joint pattern during walking [11–13].

Exoskeletons are electronically-controlled multi-joint orthoses, which may be tethered or portable. Among the tethered exoskeletons, *Lokomat* (Hokoma AG) [14] and *LOPES* (University of Twente) [15] are counted as the most prominent with gait

* Corresponding author.
E-mail addresses: rtorrealba@usb.ve (R.R. Torrealba), samueludelman@gmail.com (S.B. Udelman), edgardfr@gmail.com (E.D. Fonseca-Rojas).

http://dx.doi.org/10.1016/j.mechmachtheory.2017.05.024
0094-114X/

List of nomenclature

F	Normal contact force between each cam roller and cam disk
F_z	Vertical component of normal contact force between each cam roller and cam disk
F_θ	Horizontal component of normal contact force between each cam roller and cam disk
τ_θ	Resulting torque on a cam disk due to action of F_θ
τ_{LOAD}	External torque applied to the actuator at its output link
q_1, q_2	Angular position of main motors of the actuator
q_{r1}, q_{r2}	Angular position of cam rollers
n_1	Spur gear transmission ratio between main motors of the actuator and cam rollers
σ	Stiffness setting angle of the actuator
φ	Deflection angle of the actuator at its output link due to an external load
$s(\theta)$	Function that describes the height of the cam disk surface
θ	Positioning variable of function $s(\theta)$ with domain in $[0, 8\pi/9]$
θ_{min}	Angle θ along the cam surface that corresponds to the minimum of $s(\theta)$
r_c	Effective radius of cam disks
k	Stiffness constant of the floating spring of the actuator
z_0	Preload of the floating spring of the actuator
n_2	Bevel gear transmission ratio at the output link of the actuator
τ	Output torque of the actuator
K	Output stiffness of the actuator
q_K	Angular position of the output axis of the actuator
q_s	Angular position of the straight sided spline shaft
n_{GB1}	Transmission ratio of gearbox of the main motors of the actuator
$\dot{q}_1$, $\dot{q}_2$	Angular speed of main motors of the actuator
$\dot{\sigma}$	Position change ratio of σ
$\dot{q}_K$	Angular speed of the output axis of the actuator
V	Induced voltage of main motors of the actuator
I	Current of main motors of the actuator
k_q	Velocity characteristic constant of main motors of the actuator
k_τ	Torque characteristic constant of main motors of the actuator
R	Electrical resistance of main motors of the actuator
$\dot{q}_3$, $\dot{q}_4$	Angular speed of motors of the BLAPS
$\dot{q}_w$	Linear speed of power screw of the BLAPS
N	Number of threads of screw of the BLAPS
P	Pitch of screw of the BLAPS
n_{GB2}	Transmission ratio of pulleys system of the BLAPS
K_f	Stiffness value applied by actuator during stance flexion sub-phase of gait cycle
K_e	Stiffness value applied by actuator during stance extension sub-phase of gait cycle
W	Weight of patient
H	Height of patient
q_{BLOCK}	Angular position of miniature stepper motors of the BLAPS
σ_{min}	Minimum relative position between the cam rollers $(=0)$
σ_{max}	Maximum relative position between the cam rollers

rehabilitation purposes. These allow to use the body-weight supported treadmill training technique, which has become an established therapy to treat patients with dysfunctional gait after stroke or spinal cord injury since the 1990s [4,16–18]. This technique involves partially bearing the patient's weight through a harness, while he or she walks on a treadmill by means of applying external forces on their legs, either by therapists or a robotic device, or simply by his/her own legs movements. Initially, this was applied with a fixed gait-pattern, but further research demonstrated that gait rehabilitation was noticeably encouraged with gait pattern adaptation [7,15,19]. In [7] and [19], Jezernik et al. exploited the principle underlying the gait-pattern adaptation using the *Lokomat* in such a way that the interaction between the device and the patient is minimized, as the former follows the volitional forces exerted by the latter. Similarly, in [15], Veneman et al. aim to use a device that allows near-to-normal free walking or a wide range of possible content of training and supportive actions. In this case, the scope with the *LOPES* is open through three different operation modes: (1) patient-in-charge, (2) robot-in-charge and (3) therapist-in-charge. However, most of these treadmill training-based exoskeletons are only accessible at large rehabilitation centers or hospitals, therefore limiting their reach to patients needing this kind of therapy [20].

As for the portable exoskeletons, these enable gait assistance and training at outpatient rehabilitation centers or home settings. Several commercial models are now available, counting *Ekso* (Ekso Bionics), *REX* (REX Bionics) and *ReWalk* (ReWalk

Robotics), among others. Also, there are currently found electronically-controlled knee orthoses, such as the commercialized *Tibion Bionic Leg* (Tibion Corporation) and the *C-Brace* (OttoBock). These devices have been demonstrated to bring further improvements to gait of patients after they have reached a plateau with conventional body-weight supported treadmill training [21]. Typically, actuators utilized by such portable electronically-controlled orthoses are based on more or less sophisticated variable stiffness mechanisms (VSMs) that allow actuation on the joints in a compliant way [22–25]. This comes from the fact that walking is a process naturally accomplished by sound lower-limb joints managing interaction between soft and hard tissues to control both position and stiffness in a synchronized way during gait. Years ago, mimicking such natural behavior was out of the scope of classic robotics, for which high stiffness is paramount to ensure precise movements and ease trajectory tracking control. But more recently, a kind of actuators known as variable impedance actuators (VIAs) have undergone an amazing growing tackling soft-compliance applications [26], as robotics has spread beyond its original area of positioning control [27]. Indeed, not in vain, the VIAs are also called adjustable compliance actuators, as they seek to adapt their resistance to motion, especially when facing forces coming from the interaction with their surroundings, which is the case in exoskeletons or electronically-controlled orthoses.

Nonetheless, leaving aside weight as the main challenge of these devices to achieve portability, wearable knee orthoses seem to be limited by their intrinsically-determined response due to mechanical components selected in terms of the impedance they must provide depending on their purpose [20,22,23,25,28]. In short, impedance variability is commonly achieved in actuators by means of including at least one kind of springs in the VSM, but at the same time, this is translated into a discrete behavior given in terms of a low, medium, or high stiffness response [20,22,25,28]. This paper presents a different approach for designing a novel VIA specifically tailored to the knee joint of a portable human gait rehabilitation exoskeleton being developed by the Mechatronics Research Group (MRG) of the Simón Bolívar University, Caracas-Venezuela. In this regard, the novelty of this actuator is grounded on a specific design that grants maximum stiffness variability reachable in a continuous and smooth way, whereas the kinematic, kinetic and anthropometric requirements for the rehabilitation of the human knee joint during level walking are complied.

This paper is structured as follows: In Section 2, a biomechanical insight into both the sound and pathological knee joints is presented. Subsequently, the design criteria for the knee actuator are established in Section 3, which divides these as physiological requirements, physical constraints and mechatronic specifications. Section 4 shows the details of the mechanical design of the main mechanism of the actuator, as well as of the complimentary system developed to enhance the response of the former in terms of energy consumption. In Section 5, the mathematical modeling of the whole actuator is thoroughly explained, while Section 6 is devoted to the simulations carried out to validate the performance of the actuator. Finally, technical specifications of the actuator developed are summarized in Section 7, some comments on the implications of the results obtained from the validating simulations are discussed in Section 8, and concluding remarks are displayed in Section 9.

2. Biomechanics of knee joint

A specifically-developed actuator to assist the knee joint must interact with the impaired knee having as reference the natural biomechanics of a sound one. In particular, Fig. 1 depicts the normal human gait cycle from healthy subjects walking on level terrain, in terms of the knee muscle activation pattern and subsequent joint angle, internal moment and power. In this paper, these plots will be considered as the references to aim at in order to rehabilitate an impaired knee by means of the actuator here designed. In addition, characterization of the pathological knee joint must be also known in contrast to the sound knee behavior when walking. This yields to understand the phenomenology of the impairment and later, to identify the requirements as well as the limitations that will be faced during a gait rehabilitation therapy.

2.1. Sound knee joint

In Fig. 1, the angular range covered by the knee joint along a typical gait cycle on level terrain is observed though, of course, some variability, even among healthy subjects, must be expected. Thus, at least a range from 0–90° should be allowed by the actuator for the knee angle: ∼0–70° during the gait cycle and ∼0–90° for sitting-standing transitions. In addition, on the kinematics, there are two peaks of flexion, one during the stance and the other one during the swing. The former peak (∼20°) denotes the end of the load response after the initial contact, during which a natural damping mechanism of the leg operates to absorb the kinematic energy that brings the body from the swing. This is why it is observed an isometric contraction of the quadriceps and hamstrings around the knee, to begin deceleration of the leg even before the foot hit the floor, and afterwards, to provide stability while receiving the inertial load of the body during the stance phase initiation. The latter peak is much higher than the former (∼60–70°) and occurs toward the 70% of the gait cycle during the initial swing. This is produced by the combined contraction of the hamstrings as knee flexors, the quadriceps as hip flexors and the ilipsoas as the natural flexor of the hip; indeed, the value of this peak depends on the knee angular velocity at toe-off, which is directly related to the power peak of the hip that happens toward the end of the terminal stance subphase of the gait cycle [29]. Regarding the torque exerted by the flexor-extensor muscles, it is observed that the maximum occurs toward 12% of the gait cycle (see Fig. 1). This value was taken as the maximum torque required from the actuator in case this would have to completely assume the load for moving the knee joint, for example during the first stages of rehabilitation of a severely impaired patient. Furthermore, considering the knee angular velocity and torque, the power at

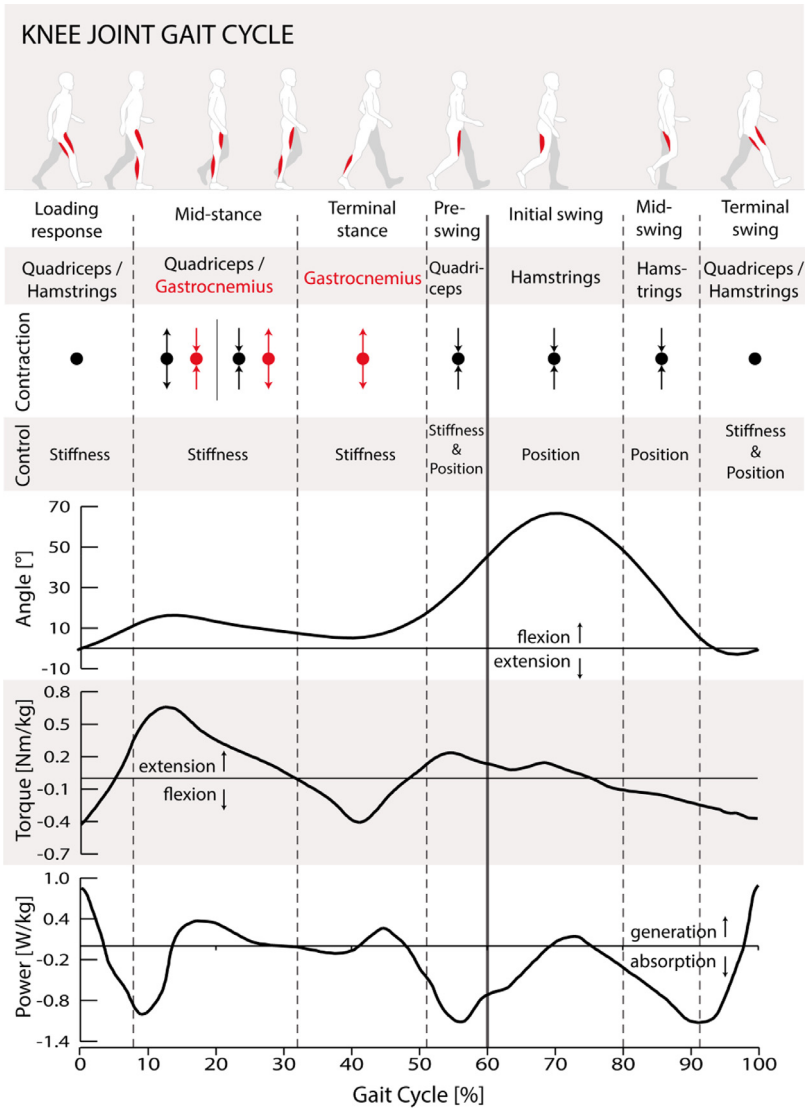

Fig. 1. Knee muscle activation pattern (arrows pointing inward mean concentric contraction, arrows pointing outward mean eccentric contraction, no arrows means isometric contraction) and typical kinematic and kinetic curves of the knee joint during level walking normalized by weight of the subject (adapted from data of [30]).

the knee joint is obtained during walking as well. As can be seen in Fig. 1, the knee joint mostly absorbs energy (negative values). In fact, there are observed three peaks of absorption, and barely activity for power generation at the joint during level walking. Such absorption mainly occurs through eccentric contraction of the quadriceps, which in terms of the actuator response refers to its intrinsic stiffness before external forces.

2.2. Pathological knee joint

Gait disorders due to neurological damage after stroke or spinal cord injury usually render absence of the correct muscle control on the legs to provide a biomechanically natural mode of locomotion. The impacts can vary from a non-desired gait pattern to the impossibility of walking due to a collapsing body [28]. In either case, it is worthy to point out why any of such degrees of impairment are observed, which is basically related to the extensor muscles of the knee, and more specifically, to their weakness. Quadriceps act during the stance phase to counterbalance the knee flexion induced by the ground reaction force after initial contact. Indeed, the higher the weakness of this muscle group, the higher the risk of falling of the patient at the end of the loading response sub-phase (see Fig. 1). Likewise, knee extensors also control the rate of knee flexion during the swing phase, which is mainly induced by the dynamics of the leg, while in the air. In this case, if the quadriceps are not responding correctly, the knee joint can flex in an uncontrolled manner, specially compromising

the reach of the full extension position before initiating the next gait cycle (see Fig. 1), which then has as the most likely ending scenario the one of a buckling knee that leads to a fall, with all the consequences this may bring. A typical way found by patients to overcome the aforesaid absence of power to extend the knee and control its flexion during stance is to keep it blocked by means of excessive hip extension and anterior trunk bending. However, neither of these strategies is biomechanically convenient; on the contrary, both can lead to a hyperextension of the knee, a condition that may end up with an anatomical deformity that later may turn into a major clinical concern, from a seemingly corrective action on the gait pattern. Finally, resuming the purpose of the actuator to be developed here, such a device must then be able, on the one hand, to compensate for the aforementioned debility of the knee extensor muscles exhibited by patients after stroke or spinal cord injury (at least in the initial stages of a gait rehabilitation therapy) [2,3], and on the other hand, to specifically exercise the knee extensors to promote their strengthening and therefore grant more physiological patterns during walking (probably after completing half or more of a gait rehabilitation process) [9,25].

3. Statement of design criteria

This section introduces a series of specifications that will guide the design process of the actuator to be developed here. In such sense, these bullet points define the design space for the actuator, by establishing some constraints, either in a compulsory or desirable way, basically in terms of minimum requirements, maximum limits, or ranges of operation expected. Hence, the background presented in the prior sections was taken into account to state the following design criteria, where both physiological requirements and physical constraints are based on a subject weighing maximum 75 kg (and maximum height of 1.9 m) walking on level terrain.

3.1. Physiological requirements

- The actuator should allow a minimum knee angular range of motion in the sagittal plane from 0 to 90°. The motion of the joint in other body planes is discarded.
- The actuator must offer torque, stiffness and maximum power of [−30, 50] N.m, [110, 500] N.m/rad and 80 W, respectively (according to Fig. 1).
- The actuator must not affect the patient's gait unfavorably in any manner.

3.2. Physical constraints

- The actuator should weigh a maximum of 3 kg, to guarantee portability of the device [20].
- The actuator should have no more than 100, 100 and 350 mm, for depth, width and length, respectively, to make the exoskeleton compact and easy to wear.
- The actuator must be attached laterally to the thigh segment of the leg, to not interfere with sitting position while the patient is wearing the device [25].

3.3. Mechatronic specifications

- The actuator should have a maximum stiffness adjusting time of 0.8 s [31].
- The minimum deflection of the actuator on either direction must be 10°, to allow the natural flexion of the knee during the load response sub-phase of the gait cycle.

4. Mechanical design of actuator

4.1. BAFSA

An actuator design emerged from combining the FSJ (Floating Spring Joint) [32] and BAVS (Bidirectional Antagonistic Variable Stiffness) [33] models; such actuator was named BAFSA, being this a Bidirectional Antagonistic Floating Spring Actuator, as shown in Fig. 2. Both FSJ and BAVS models brought out from the VIACTORS consortium [34] have very different features, especially regarding motor size. The FSJ is featured by two motors of significantly different size, one dedicated to setting the position of the joint (the big one) and the other one devoted to change the stiffness preset at the joint (the small one). The BAVS, on the other hand, comprises two motors of the same size, which sum their torques through the VSM at the output, whereas stiffness is varied by the relative motion between both.

By combining the FSJ and BAVS models as presented in this work, an actuator with a highly convenient slender structure suitable to be attached along the thigh segment of an exoskeleton was designed, as well as its cam shape and other parameters to make the output compliant with the design specifications previously established. For creating an actuator targeted at the knee joint, it was not feasible to scale one of the aforementioned models, or any other VIA known so far. In terms of output, the ranges of operation would not have fitted in a conveniently-correlated way; specially the torque-stiffness relationship is very sensible to design parameters [35], and those actuators were developed for different applications. Moreover, as for the mass and volume, simply scaling other VIA would have resulted in a power-to-mass, power-to-volume, maximum

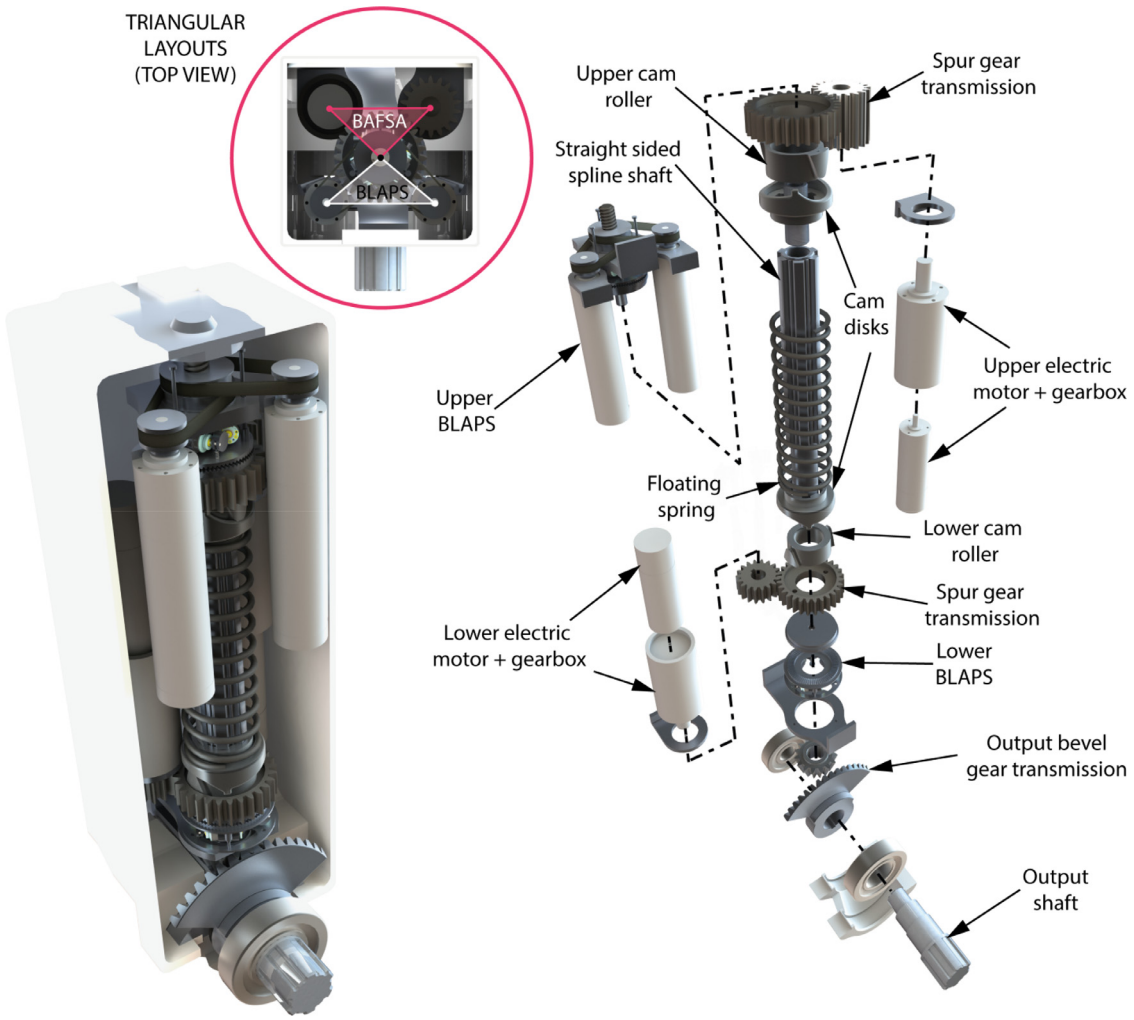

Fig. 2. Mechanism and components of the BAFSA. Notice the triangular layout in the top view encircled.

torque-to-mass and maximum torque-to-volume ratios inappropriate for the knee joint, for the same reasons just stated [26].

For the sake of compactness, the BAFSA presents a triangular layout: there is a straight-sided spline (SSS) shaft in one of the vertices, and one electric motor in each of the other two, all axially aligned as seen encircled in Fig. 2. On each end of the shaft, there is a cam disk coupled through the straight-sided splines (this feature comes from the BAVS model), as well as a cam roller connected to one of the electric motors through a spur gear transmission. The shaft continues outward on one of its ends, fixing a bevel pinion whose crown (output bevel gear transmission) is connected to the output shaft of the actuator.

As the cam rollers are not fixed to the shaft, when the motor turns, it makes the corresponding cam roller slide over the cam disk, producing an axial displacement of the latter along the SSS shaft. Such displacement renders at the same time a compression load on the floating spring located between both cam disks (this feature comes from the FSJ model), and thus, part of the reaction force exerted by the floating spring on them is transmitted to the shaft in terms of torque (through the cam disks), as shown in Fig. 3 (see components F_θ). Basically, this is how the VSM of the BAFSA works; therefore, the cam surface shape is determinant for the range of stiffness variability. A very detailed focus was done in this regard, resulting an optimal cam design by using cubic Bézier curves to parameterize the surface shape, and a differential evolution algorithm to seek for the best curve in terms of maximizing the range of stiffness variability, according to the specifications and components of the BAFSA. The details on the design of the cam shape were disclosed in [35].

On the functioning, the motors are axially counter-mounted (see Fig. 2). That is, when they rotate in the same direction, they are actually inputting power on the cam rollers in opposed directions. This is called *normal mode*: the higher the spring compression, the higher the stiffness offered by the actuator before external forces. Conversely, when the motors rotate in the opposing direction, both cam rollers rotate in the same direction, making the output shaft rotate with them. This is

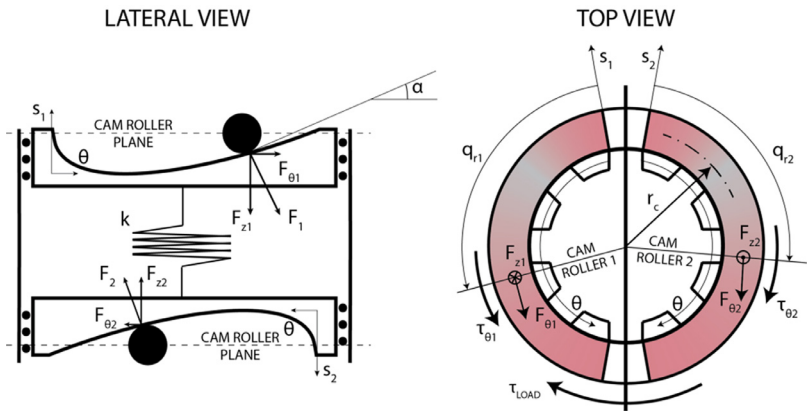

Fig. 3. Model of the BAFSA in 2D: at the left (lateral view), the model represents the cam rollers fixed in their motion planes (by the motors), while the cam disks and the floating spring can move vertically along the SSS shaft depending on the forces F_{z1} and F_{z2} and the spring constant k; at the right (top view), the forces $F_{\theta 1}$ and $F_{\theta 2}$ exerted on the cam disks turn out in the resulting torques $\tau_{\theta 1}$ and $\tau_{\theta 2}$ produced by the VSM of the BAFSA. Note that each half of the top view represents a cam disk, and the coordinates q_{r1} and q_{r2} point out the angular position of the corresponding cam roller. In addition, notice that the external torque applied to the actuator τ_{LOAD} is illustrative, as it can actually go in either direction (adapted from [35]).

called *helping mode*, in which the BAFSA works to vary the angular position of the joint through the output bevel gear transmission. Note that in either operation mode, compression of the spring can be modulated both in displacement and velocity. For instance, both cam rollers may be rotating in the same direction but at different speeds; therefore, both the angular position and stiffness offered at the output link of the BAFSA would be changing simultaneously.

4.2. BLAPS

To enhance the versatility of the BAFSA to regulate its energy consumption, a complementary system was also designed to vary the preload stiffness automatically, whereas allowing output link deflection without demanding further power from the actuator motors. Such a module was called BLAPS (blocking and axial positioning system). The blocking module acts as a brake of the cam rollers and thus, the stiffness at the joint results physically independent of the energy input by the BAFSA motors once this module is engaged, allowing passive deflection of the knee joint. In other words, the blocking function of the BLAPS enables the BAFSA to sustain a given stiffness at no energy cost, making it an intrinsically energy-efficient actuator [36]. The axial positioning module, on the other hand, alters the stiffness range of operation by setting the axial position of one of the cam rollers (the one opposed to the output link), while the other remains axially fixed, thus changing the preload of the floating spring.

The BLAPS is depicted in Fig. 4. As aforesaid, the blocking function is associated to each cam roller, whereas the axial positioning one is only applied to the end opposed to the output link (upper BLAPS). Each of the blocking mechanisms is implemented through a brake, consisting of a couple of radial spline disks that immobilize the corresponding cam roller when engaged. More in detail, one of the radial spline disks is attached to the spur gear and, in consequence, to the corresponding cam roller, and the other one is rotationally constrained, through the bars on the upper BLAPS (see the exploded view in Fig. 4) and directly by the chassis on the lower one, hence resulting the blocking when both disks are engaged. For doing so, three eccentric cams push both disks together by means of three miniature stepper motors, respectively. For smoothing the disk engagement, a particular coupling is achieved through a compression spring located between each cam and the blocking disk (see the zoomed view in Fig. 4). Each of these springs absorbs rotation of its corresponding cam as axial compression, to reduce impact between the spline tops when engaging the brake. Conversely, for disengaging the brake, the cams are separated from the blocking disk and a set of three tension springs bring it back to its original position. Regarding the axial positioning function, this is achieved through a bearing-mounted nut, which is threaded over a power screw that moves the corresponding cam roller axially (see the exploded view in Fig. 4); thus, the preload of the floating spring is varied and subsequently, the stiffness offered by the BAFSA at its output. Power is transmitted from the electric motors to the nut by a transmission of two synchronous belts and pulleys. The motors are similar to the main ones of the BAFSA, conforming another triangular layout as observed in the top view of the actuator encircled in Fig. 2.

5. Mathematical modeling of actuator

5.1. BAFSA

The coupling of the cam disks through the floating spring entails a term denoted as σ, known as the stiffness setting angle of the actuator and given by Eq. (1) in terms of the position of the motors, q_1 and q_2, seen directly on the cam rollers

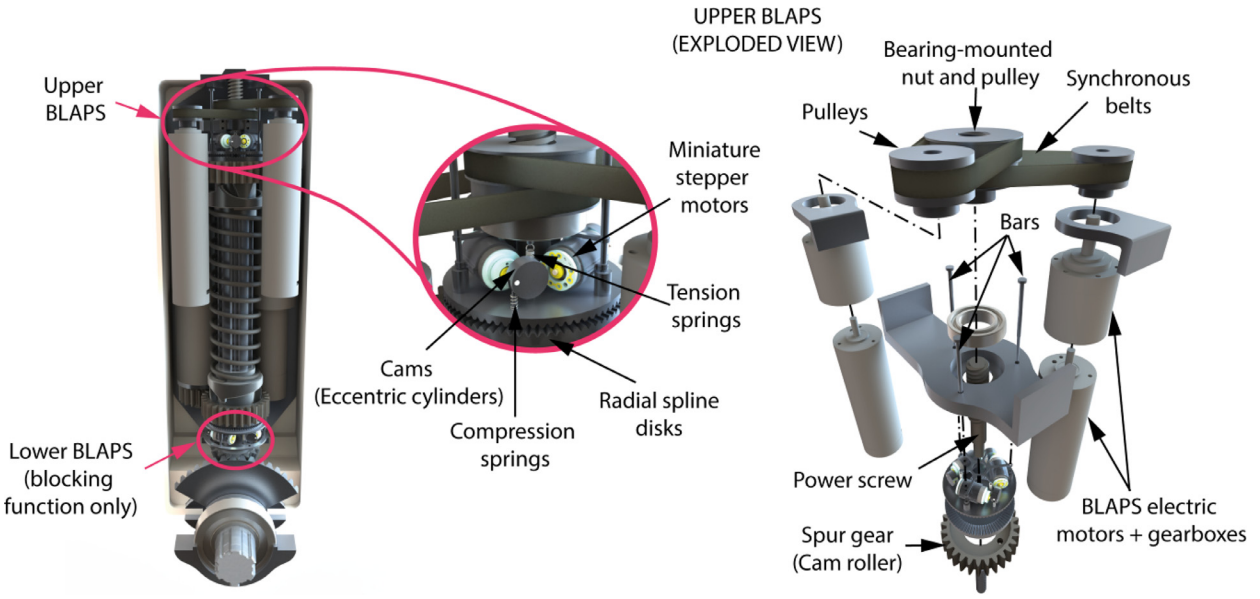

Fig. 4. Mechanism and components of the BLAPS. Notice the details on the upper BLAPS: the zoomed view in the center and the exploded view at the right.

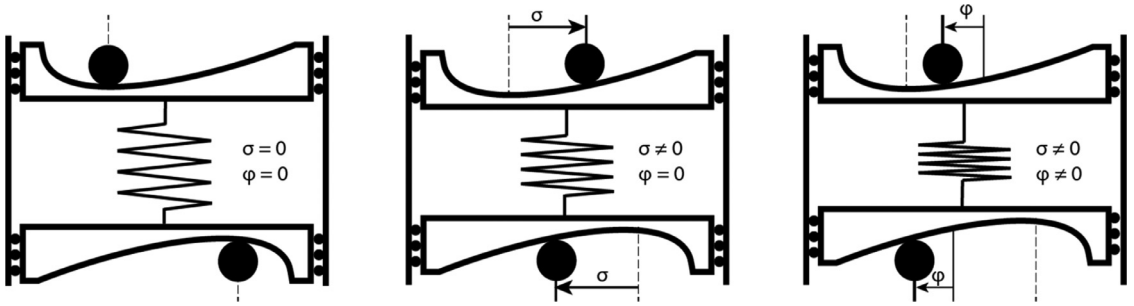

Fig. 5. Model of the BAFSA in 2D showing the θ decomposition in terms of σ and φ: as the model is in 2D, σ and φ are represented as linear displacements, but actually they are angular displacements (rotations), as was shown for the θs in the top view of Fig. 3.

as q_{r1} ($=n_1 \bullet q_1$) and q_{r2} ($=n_1 \bullet q_2$) – i.e., transformed through the spur gear transmission ratio n_1 (see Fig. 2).

$$\sigma = (q_{r1} + q_{r2})/2 \tag{1}$$

Similarly, the deflection observed at the output of the VSM of the actuator before an external load is given by φ. Then, the output torque of the actuator can be written as in Eq. (2), including σ and φ in accordance to the functioning model of the BAFSA shown in Fig. 5. θ_{min} is the angle θ along the cam surface that corresponds to the minimum of $s(\theta)$, which is the function that describes the height of the cam surface, with $\theta \in [0, 8\pi/9]$. In addition, r_c is the effective radius of the cam disks (see Fig. 3), k is the constant of the floating spring, z_0 is its preload, and n_2 is the output bevel gear transmission ratio (see Fig. 2).

$$\tau = \left\{ r_c \cdot k \cdot \left[s(\theta_{min} + \sigma + \varphi) + s(\theta_{min} + \sigma - \varphi) + z_0 \right] \cdot \left[s'(\theta_{min} + \sigma + \varphi) - s'(\theta_{min} + \sigma - \varphi) \right] \right\} / n_2 \tag{2}$$

Eq. (2) sets the torque-deflection relationship for a given angle σ, thus the slope of the curves of such relationship corresponds to the stiffness of the actuator $K(\sigma, \varphi)$, expressed as in Eq. (3). Fig. 6 presents the resulting cam shape from [35], as well as the intrinsic torque-deflection and stiffness-torque relationships of the BAFSA.

$$K(\sigma, \varphi) = \partial \tau / \partial \varphi \tag{3}$$

Finally, the characteristic equation of the VSM of the BAFSA can be expressed as in Eq. (4) on any of the cam rollers ($i = 1,2$). Thus, the deflection φ is computed by calculating σ from Eq. (1) and measuring the angular position of the cam rollers, q_{r1} or q_{r2}, and the angular position of the knee, q_K ($=n_2 \bullet q_s$), through encoders attached to the output axis of the motors and the actuator, respectively.

$$q_{ri} = q_s + \sigma + \varphi; \quad i = 1, 2 \tag{4}$$

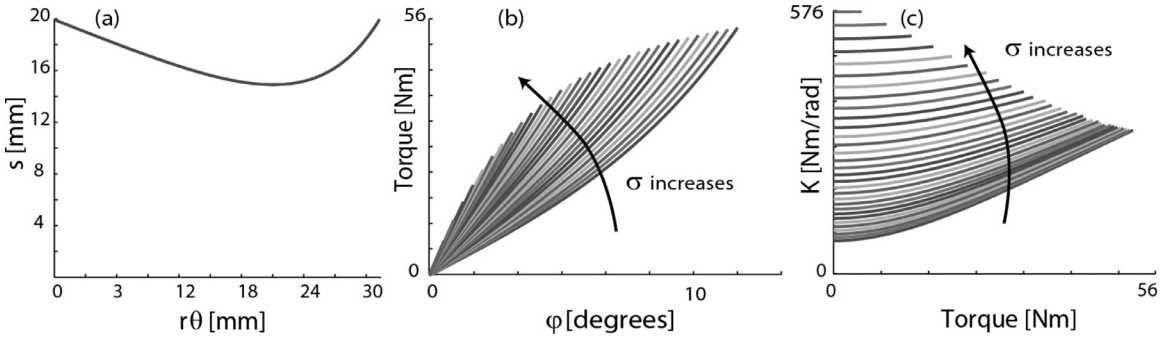

Fig. 6. Characteristic curves of the BAFSA: (a) cam profile, (b) torque-deflection relationship, and (c) stiffness-torque relationship. Considering the gear ratio of 1:3 introduced by the output bevel gear transmission of the BAFSA (see Fig. 2), both torque and stiffness resulting from the VSM are amplified: the former, 3 times, while the latter, 9 times – going from 0 to 56.25 N.m and from 126 to 576 N.m/rad, respectively (adapted from [35]).

Table 1
Main components of the BAFSA.

Component	Parameter	Description	Model
Motor 1–2	q_1, q_2	Angular position of spur	Maxon EC
Encoder		gear connected to motor	22–100W
Gearbox	n_{GB1}	Planetary 4 stages 1:246	Maxon
Spur gears	n_1	Transmission ratio 18:28	–
Output link	q_K	Knee angular position	–
Encoder			
Bevel gears	n_2	Transmission ratio 1:3	–
Motor 3–4	q_3, q_4	Angular position of	Maxon EC
Encoder		BLAPS driving nut	22–120W
Gearbox	n_{GB2}	Planetary 2 stages 1:12.76	Broadway
Synchronous belts and pulleys	n_3	Transmission ratio 1:1.6	–
Motor 5–10	q_{BLOCK}	Angular position of	Faulhaber
Encoder		BLAPS cams	AM0820

On the other hand, assuming that both torque τ and stiffness K are known at the output link of the actuator for a given patient (physiological requirements) and rehabilitation strategy (therapist prescription), a two equation system composed of Eqs. (2) and (3) is solved to obtain σ and φ having fixed z_0 (see Fig. 6(b) and (c)), and then, the torque of each motor can be calculated from Eqs. (4), (5) and (6), being the transmission ratio of the gearbox of the motors defined as n_{GB1} (see Table 1). As for the angular speed of each motor, $\dot{q}_1$ and $\dot{q}_2$, these are determined from Eqs. (7) and (8), respectively. These equations express the addition of the angular speed at the output link of the actuator to meet a normal gait, $\dot{q}_K$, to the relative speed of the cam rollers sliding over the cam disks, which is the position change ratio $\dot{\sigma}$.

$$\tau_1 = r_c \cdot k \cdot n_1 \cdot n_{GB1} \cdot \left[s(q_{r1}) \cdot s'(q_{r1}) + s(q_{r2}) \cdot s'(q_{r1}) + z_0 \cdot s'(q_{r1}) \right] \tag{5}$$

$$\tau_2 = -r_c \cdot k \cdot n_1 \cdot n_{GB1} \cdot \left[s(q_{r1}) \cdot s'(q_{r2}) + s(q_{r2}) \cdot s'(q_{r2}) + z_0 \cdot s'(q_{r2}) \right] \tag{6}$$

$$\dot{q}_1 = \dot{q}_K / (n_1 \cdot n_2 \cdot n_{GB1}) + \dot{\sigma} / (2 \cdot n_2) \tag{7}$$

$$\dot{q}_2 = \dot{q}_K / (n_1 \cdot n_2 \cdot n_{GB1}) - \dot{\sigma} / (2 \cdot n_2) \tag{8}$$

With this, considering the equations for DC motors that relate induced voltage V and current I with velocity $\dot{q}$ and torque τ, the output power for each motor i can be computed for every instant j along the gait cycle from Eqs. (9)–(11), where k_q and k_τ are the characteristic constants of the motors for velocity and torque, respectively, while R is their electrical resistance. Lastly, the total power is the sum of the power of the two motors and then, the estimation of energy consumption is obtained by numerical integration of the total power (in absolute value) over time.

$$V_i^j = \dot{q}_i^j / k_q \tag{9}$$

$$I_i^j = n_1 \cdot \tau_i^j / k_\tau \tag{10}$$

$$P_i^j = I_i^j \cdot V_i^j + I^{2j}_i \cdot R \tag{11}$$

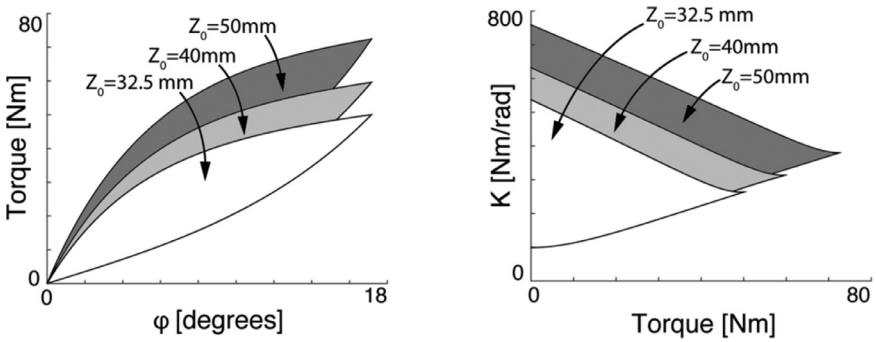

Fig. 7. Further ranges of torque-deflection and stiffness-torque relationships enabled by the BLAPS.

5.2. BLAPS

The axial positioning function of the BLAPS achieved through the bearing-mounted nut rotation implicates a speed conversion that turns the angular speed of the motors, $\dot{q}_3$ and $\dot{q}_4$, which are equal being both motors coupled to the same pulley (see Fig. 4), into a linear speed of the power screw, $\dot{q}_w$, as given by Eq. (12). N is the number of threads of the screw, P is its pitch, n_{GB2} is the transmission ratio of the gearbox of the motors and n_3 is the transmission ratio of the pulleys system (between the output of the gearbox of the motors and the nut). The original design of the BAFSA, from which the plots shown in Fig. 6 were obtained, corresponded to a preload z_0 of 40 mm; afterwards, by introducing the BLAPS, a range from 32.5 to 50 mm was admitted. This broadened the operating range as depicted in Fig. 7 in terms of torque and stiffness now on the BAFSA.

$$\dot{q}_w = N \cdot P \cdot \dot{q}_i / (2 \cdot \pi \cdot n_{GB2} \cdot n_3); \quad i = 3, 4 \tag{12}$$

6. Performance simulation of actuator

Taking into account the components of the BAFSA shown in Table 1, numerical simulations were run to estimate its behavior along the gait cycle on level terrain, in terms of power and resulting energy consumption, for individuals ranging between 50–75 kg of weight and 1.5–1.9 m of height, and considering a range of 32.5–50 mm for the preload of the floating spring z_0 (according to the dimensions of the BAFSA). Particularly, regarding the range of z_0, lower values did not resemble a natural biomechanical gait and higher ones exceeded the capacity of the motors. On the other hand, although control strategies are not within the focus of this paper, setting a given level of stiffness on the BAFSA was required to perform the aforesaid simulations along the gait cycle. In this sense, the gait cycle was divided in the following sub-phases in terms of the knee angle (different to sub-division depicted in Fig. 1): stance flexion, stance extension, pre-swing, swing flexion and swing extension [37]. Then, a quasi-stiffness approach was suggested for the first two sub-phases [22], whereas the minimum stiffness corresponding to σ_{min} was applied during the swing flexion (see Fig. 6c); for the pre-swing and swing extension sub-phases, a linear transition was implemented between the stiffness values of the adjacent sub-phases. In particular, Eqs. (13) and (14) were applied for the quasi-stiffness approach in stance flexion (K_f) and in stance extension (K_e). In both equations, W refers to the weight of the patient in kg, while H regards the height in m, returning the corresponding K in N.m/rad [22].

$$K_f = 6.30 \cdot W \cdot \sqrt{H^3} - 7.93 \cdot W \cdot \sqrt{H} - 7.88 \cdot W \cdot H + 13.65 \cdot W + 33 \tag{13}$$

$$K_e = 5.91 \cdot W \cdot \sqrt{H^3} - 10.09 \cdot W \cdot \sqrt{H} - 2.85 \cdot W \cdot H + 7.35 \cdot W + 56 \tag{14}$$

6.1. Power

Simulations on the power performance of the BAFSA were carried out with a twofold purpose: on the one hand, to study the contribution of the different electro-mechanical components in its output, and on the other, to quantify the power requirement on each motor and therefore, to prove the feasibility of the design. Fig. 8 shows the normal gait power throughout the gait cycle for the most demanding case: the heaviest and tallest patient (75 kg and 1.9 m), plus the minimum preload z_0 (32.5 mm), besides the power supplied by each motor to yield such performance (see Fig. 1). The elastic power associated with the floating spring plays an important role between the load response and midstance sub-phases, and later in a minor way, toward late terminal stance and during the pre-swing. Such elastic power basically follows the behavior of the normal gait power, especially during the stance phase. This means that the floating spring contribution modulated by the motors is crucial to the output power response of the BAFSA. In this sense, negative output power means that the system is absorbing energy, which is stored by compressing the floating spring, and conversely, when the output power is positive, the

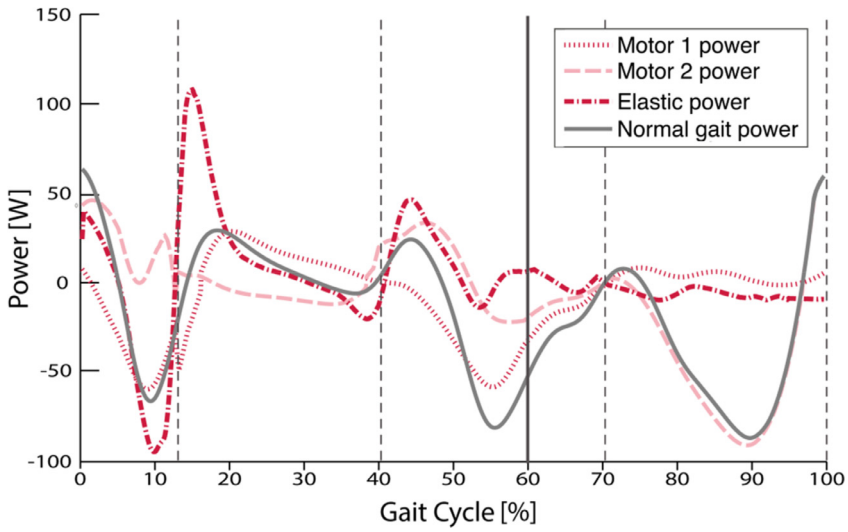

Fig. 8. Power distribution into the BAFSA for a patient of 75 kg (weight) and 1.9 m (height). Note that a change of sign in the motors power represents a change of motion direction.

Table 2
Technical specifications of the BAFSA (+ BLAPS).

Property	Unit	Value
BAFSA (+ BLAPS)		
Power	[W]	200
Peak torque	[N.m]	72
Maximum deflection	[°]	18
Stiffness adjusting time	[ms]	495
Weight	[kg]	2.964
Dimensions: L × W × T	[mm]	310 × 95 × 91
BLAPS		
Weight	[kg]	0.559
Preload adjusting time	[ms]	184

system is delivering energy, which is then returned from the floating spring. On the other hand, there are also periods in which the output of the BAFSA depends almost completely on the motors, as the spring contribution is very negligible – i.e., between midstance and late stance, and during the swing phase (20–40% and 60–100% of the gait cycle, respectively). In addition, it can be observed the wide margin that results between the maximum power of ~100 W, required for reproducing a normal gait cycle for the most demanding case (see Fig. 8), and the maximum power available from the motors of 200 W (see Table 2). Such behavior is remarkable as it is expected that an impaired knee demands more power from the system, although the measure in which this occurs will depend on the level of knee atrophy presented by the patient [20,28].

6.2. Energy consumption

Energy consumption was estimated taking into account normal torque and walking speeds for individuals in the aforementioned range and varying the spring preload z_0, in order to explore the energy requirements of the BAFSA when coping with a wide variability in anthropometric parameters, and to rate the contribution of the BLAPS towards fixing a set-point for operation of the actuator during a particular therapy, respectively. In general, the results showed that the highest the preload z_0, the less the energy cost for the BAFSA, as seen in Fig. 9. However, it is not possible to set the highest preload for every patient as this has influence in the stiffness range, as shown in Fig. 7. More in detail, there are also observed distinct behaviors of the energy consumption of the actuator between individuals of different heights for a given preload and the minimum and maximum weights considered. Thus, the simulated model allowed to appraise the capabilities of the BAFSA in terms of energy consumption. As a matter of fact, the energy consumption of the BAFSA for the most demanding case defined before would be 52.91 J per gait cycle, as a first approximation (no friction forces or dynamical effects on the internal components of the actuator are being included so far). It is estimated that an average person (with no gait impairment) takes between 2,500 and 7,500 strides per day [29]; hence, the amount of energy reported for the BAFSA per gait cycle is traduced into a range of 132,275 – 396,825 J per day. Of course, a person requiring knee rehabilitation will not take as many strides per day, but such a range gives an idea of the energy that would be demanded from the batteries per rehabilitation session or simply on a daily basis. In addition, an approximation to the maximum stiffness adjusting time of the VSM of

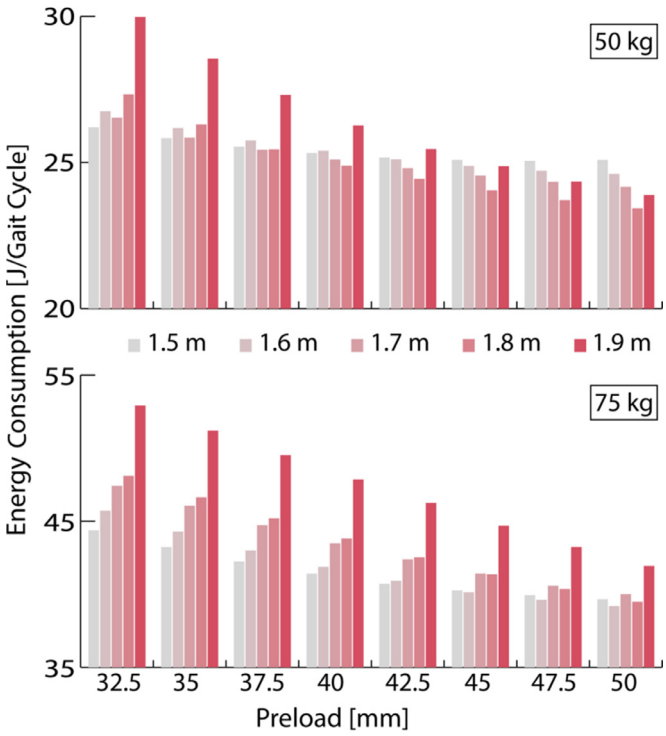

Fig. 9. Energy consumption of the BAFSA per normal gait cycle varying the spring preload z_0 and the height of the patients for the minimum and maximum weights considered: 50 and 75 kg, respectively.

the BAFSA was obtained from a simulation of the dynamic system where the change from $\sigma_{min}(=0)$ to σ_{max} was evaluated, being σ_{max} the maximum relative position between the cam rollers, which is achieved at zero output torque τ and zero deflection angle φ. Thus, the maximum stiffness adjusting time of the VSM was estimated in 0.495 s (2% criterion). Similarly, it was also estimated a maximum preload adjusting time of 0.184 s through the BLAPS.

7. Technical specifications

From the outcomes shown above in this work, the technical specifications of the BAFSA are summarized in Table 2. Likewise, it is worthy to point out the resulting ratios of the BAFSA relating power and torque with mass and volume. The BAFSA has a power-to-mass ratio of 67.48 W/kg, a power-to-volume ratio of 74.63 W/l, maximum torque-to-mass ratio of 24.29 N.m/kg, and maximum torque-to-volume ratio of 26.87 N.m/l. In this regard, the reader is invited to go over the work of Tagliamonte et al. [26] in order to locate the BAFSA within the family of VIAs, although it is not the intention to establish any comparison, since it is known that the suitability of a VIA depends on its particular application.

8. Discussion

A rehabilitation process could be very variant, mostly depending on the pathology and the degree of atrophy exhibited by the impaired knee. This is traduced in a demand of a wide range of stiffness variability by the actuator destinated to cope with such a treatment, which is precisely the main characteristic of the BAFSA, that furthermore can apply a sustained level of stiffness without consuming additional power from its motors, thanks to the assistance of the BLAPS. Thus, the actuator here developed is suitable to implement different therapeutic strategies on the impaired knee joint, which could mean going from a *high impedance* behavior, to impose specific movements or offering resistance to exercise weakened muscles, until a *low impedance* response, in order to avoid hurdling the motion of the knee imposed by the wearer, for example at the terminal stage of a given therapy [20,22,25].

The ranges of parameters selected to perform the validation of the actuator pretend to show enough evidence on its versatility to modulate its stiffness along the gait cycle [35], and with this, to set the basis for the proposal and testing of suitable control strategies to be applied on the BAFSA [5,6,9,18,19,21]. As for the preload z_0, in practice, this might be modulated for offering a given stiffness at the output link of the actuator, rather than for saving energy. In other words, even though certain range of z_0 may be not energy efficient, this could be needed in order to grant the stiffness range demanded by specific exercises on particular patients [5,8,9,18]. For this, a preset coarse stiffness level may be applied, from which then to modulate the stiffness more precisely along the gait cycle, in accordance to the rehabilitation therapy

in course, by combining the functions of the VSM of the BAFSA and the BLAPS. At the end, it will depend on the control applied on the BAFSA, whether the preload (through the BLAPS), the stiffness (through the VSM), or both, are modulated real-time during a therapy session.

Finally, from the outcomes of the simulations carried out in this work, a soft-hybrid position-stiffness control strategy is foreseen for the actuator aiming at restoring functionality of the impaired knee joint for walking. With such intention, the stiffness reference would be handled dually, either automatically, mode (1) robot-in-charge, or externally, mode (2) therapist-in-charge, during a therapy [2,20,25]. In this regard, positioning is included in the control because active participation of the patient in gait retraining does not mean the absence of a physiological reference trajectory for the joints being treated [38]. On the contrary, the retraining concept implicates that the neurological circuits of the affected joint must relearn, and for doing this, a regular physiological motion reference is needed as a prerequisite for skill acquisition [39]. Therefore, rehabilitation devices devoted to restore natural mobility of impaired joints during gait must generate the corresponding reference trajectories in an autonomous way, and impose them to the patient's joints in a lower or higher degree depending of the deviations observed from these and on the level of stiffness being applied.

9. Concluding remarks

This paper presents the design of a variable impedance actuator specifically oriented to its application at the knee joint of a lower-limb rehabilitation exoskeleton. Such design combines the FSJ and BAVS models, previously introduced in the literature, to create a new one, called BAFSA, with specific features that make it particularly suitable for the rehabilitation of the knee joint. In this sense, the natural knee performance along the gait cycle was taken into account for the conception, besides the characterization of the pathological knee. The design was presented in a thorough way, emphasizing the functioning of the system supported on its mathematical modeling. Particularly, the BAFSA is conceived to operate on a portable exoskeleton, which maximizes the efficacy of the gait rehabilitation in comparison to the one executed on treadmills and eases its application on daily life activities and in outdoors. In this sense, the implementation of the BAFSA was tackled by means of simulations reproducing a normal gait cycle on level terrain in terms of power and energy consumption. It was found that the BAFSA has twice the power required even for the most demanding case studied during level walking for reproducing a normal gait cycle. This leaves a good margin available considering that an impaired knee will demand a higher amount of power and energy consumption for rehabilitation, depending on the level of atrophy of the knee joint treated and the assisstive therapy applied. In this regard, it is recommended to apply the highest preload in favor of energy saving, but always bearing in mind that it is of paramount importance a prior assessment of the admissible stiffness at the knee joint of the patient, in order to not affect him or her in any unfavorable way. In regards to future work, the fabrication of a BAFSA prototype still remains, in order to materialize the design here presented and test any control strategy proposed for a given rehabilitation therapy. On the other hand, from the technical specifications fulfilling the initially established design criteria, it can be also claimed that the BAFSA is suitable to power knee orthoses in general, and the BLAPS is feasible to be introduced into particular VIAs, to enable the setting of a given level of stiffness without demanding further power from the actuator motors to maintain it.

References

[1] H.K. Kwa, J. Noorden, M. Missel, T. Craig, J. Pratt, P. Neuhaus, Development of the IHMC mobility assist exoskeleton, in: Proceedings of the IEEE International Conference on Robotics and Automation, Kobe-Japan, 2009, pp. 2556–2562.
[2] S.K. Agrawal, S. Banala, K. Mankala, V. Sangwan, J. Scholz, V. Krishnamoorthy, W. Hsu, Exoskeletons for gait assistance and training of the motor impaired, in: Proceedings of the IEEE International Conference on Rehabilitation Robotics, Noordwijk-The Netherlands, 2007, pp. 1108–1113.
[3] D. Ferris, G. Sawicki, A. Domingo, Powered lower limb orthoses for gait rehabilitation, Top. Spinal Cord Inj. Rehabil. 11 (2005) 34–49.
[4] P. Sale, M. Franceschini, A. Waldner, S. Hesse, Use of the robot assisted gait therapy in rehabilitation of patients with stroke and spinal cord injury, Eur. J. Phys. Rehabil. Med. 48 (2012) 111–121.
[5] B. Husemann, F. Muller, C. Krewer, S. Heller, E. Koenig, Effects of locomotion training with assistance of a robot-driven gait orthosis in hemiparetic patients after stroke: a randomized controlled pilot study, Stroke 38 (2007) 349–354.
[6] L.L. Cai, A.J. Fong, C.K. Otoshi, Y. Liang, J.W. Burdick, R.R. Roy, V.R. Edgerton, Implications of assist-as-needed robotic step training after a complete spinal cord injury on intrinsic strategies of motor learning, J. Neurosci. 26 (2006) 10564–10568.
[7] S. Jezernik, R. Schärer, G. Colombo, M. Morari, Adaptive robotic rehabilitation of locomotion: a clinical study in spinally injured individuals, Spinal Cord 41 (2003) 657–666.
[8] R. Teasell, J. Bitensky, K. Salter, N.A. Bayona, The role of timing and intensity of rehabilitation therapies, Top. Stroke Rehabil. 12 (2005) 46–57.
[9] M. Mirbagheri, C. Tsao, E. Pelosin, W. Rymer, Therapeutic effects of robotic-assisted locomotor training on neuromuscular properties, in: Proceedings of the IEEE International Conference on Rehabilitation Robotics, Chicago-USA, 2005, pp. 561–564.
[10] G. Kwakkel, R.C. Wagenaar, T.W. Koelman, G.J. Lankhorst, J.C. Koetsier, Effects of intensity of rehabilitation after stroke, A research synthesis, Stroke 28 (1997) 1550–1556.
[11] R. Ham, T. Sugar, B. Vanderborght, K. Hollander, D. Lefeber, Compliant actuator designs, IEEE Robot. Autom. Mag. 16 (2009) 81–94.
[12] H. van der Kooij, J.F. Veneman, R. Ekkelenkamp, Design of a compliantly actuated exoskeleton for an impedance controlled gait trainer robot, in: Proceedings of the IEEE/EMBS Annual International Conference, New York-USA, 2006, pp. 189–193.
[13] S. Migliore, E. Brown, S. DeWeerth, Biologically inspired joint stiffness control, in: Proceedings of the IEEE International Conference on Robotics and Automation, Barcelona-Spain, 2005, pp. 4508–4513.
[14] S. Jezernik, G. Colombo, T. Keller, H. Frueh, M. Morari, Robotic orthosis Lokomat: a rehabilitation and research tool, Neuromodulation 6 (2003) 108–115.
[15] J.F. Veneman, R. Kruidhof, E.E.G. Hekman, R. Ekkelenkamp, E.H.F. van Asseldonk, H. van der Kooij, Design and evaluation of the LOPES exoskeleton robot for interactive gait rehabilitation, IEEE Trans. Neural Syst. Rehabil. Eng. 15 (2007) 379–386.
[16] S. Hesse, C. Bertelt, M.T. Jahnke, A. Schaffrin, P. Baake, M. Malezic, K.H. Mauritz, Treadmill training with partial body weight support compared with physioteraphy in nonambulatory hemiparetic patients, Stroke 26 (1995) 976–981.

[17] G. Colombo, Treadmill training with robotic orthosis Lokomat: new technical features and results from multi-center trial in chronic spinal cord injury, Int. J. Rehabil. Res. 27 (2004) 92–93.
[18] A.L. Behrman, S.J. Harkema, Locomotor training after human spinal cord injury: a series of case studies, Phys. Ther. 80 (2000) 688–700.
[19] S. Jezernik, G. Colombo, M. Morari, Automatic gait-pattern adaptation algorithms for rehabilitation with 4-DOF robotic orthosis, IEEE Trans. Robot. Autom. 20 (2004) 574–582.
[20] G. Chen, P. Qi, Z. Guo, H. Yu, Mechanical design and evaluation of a compact portable knee-ankle-foot robot for gait rehabilitation, Mech. Mach. Theory 103 (2016) 51–64.
[21] N.N. Byl, Mobility training using a bionic knee orthosis in patients in a post-stroke chronic state: a case series, J. Med. Case Rep. 6 (2012) 216.
[22] K. Shamaei, P.C. Napolitano, A.M. Dollar, A quasi-passive compliant stance control knee-ankle-foot orthosis, in: Proceedings of the IEEE International Conference on Rehabilitation Robotics, Seattle-USA, 2013, pp. 1–6.
[23] K. Kong, J. Bae, M. Tomizuka, A compact rotary series elastic actuator for knee joint assistive system, in: Proceedings of the IEEE International Conference on Robotics and Automation, Anchorage-USA, 2010, pp. 2940–2945.
[24] T. Yakimovich, J. Kofman, E.D. Lemaire, Design and evaluation of a stance-control knee-ankle-foot orthosis knee joint, IEEE Trans. Neural Syst. Rehabil. Eng. 14 (2006) 361–369.
[25] J.E. Pratt, B.T. Krupp, C.J. Morse, S.H. Collins, The RoboKnee: an exoskeleton for enhancing strength and endurance during walking, in: Proceedings of the IEEE International Conference on Robotics and Automation, New Orleans-USA, 2004, pp. 2430–2435.
[26] N.L. Tagliamonte, F. Sergi, D. Accoto, G. Carpino, E. Guglielmelli, Double actuation architectures for rendering variable impedance in compliant robots: a review, Mechatronics 22 (2012) 1187–1203.
[27] B. Vanderborght, A. Albu-Schäeffer, A. Bicchi, E. Burdet, D. Caldwell, R. Carloni, M. Catalano, G. Ganesh, M. Garabini, M. Grebenstein, G. Grioli, S. Haddadin, A. Jafari, M. Laffranchi, D. Lefeber, F. Petit, S. Stramigioli, N. Tsagarakis, M. van Damme, R. van Ham, L.C. Visser, S. Wolf, Variable impedance actuators: moving the robots of tomorrow, in: Proceedings of the IEEE/RSJ International Conference on Intelligent Robots and Systems, Vilamoura-Portugal, 2012, pp. 5454–5455.
[28] A. Cullel, J.C. Moreno, E. Rocon, A. Forner-Cordero, J.L. Pons, Biologically based design of an actuator system for a knee-ankle-foot orthosis, Mech. Mach. Theory 44 (2009) 860–872.
[29] C. Kirtley, Clinical gait analysis, in: Theory and Practice, first ed., Churchill Livingstone Elsevier, 2006, p. 316.
[30] D.A. Winter, in: Biomechanics and Motor Control of Human Movement, second ed., John Wiley and Sons Inc., Hoboken, 1990, p. 370.
[31] M. Cestari, D. Sanz-Merodio, J.C. Arevalo, E. García, An adjustable compliant joint for lower-limb exoskeletons, IEEE/ASME Trans. Mechatron. 20 (2015) 889–898.
[32] S. Wolf, O. Eiberger, G. Hirzinger, The DLR FSJ: energy based design of a variable stiffness joint, in: Proceedings of the IEEE International Conference on Robotics and Automation, Shanghai-China, 2011, pp. 5082–5089.
[33] W. Friedl, H. Höppner, F. Petit, G. Hirzinger, Wrist and forearm rotation of the DLR hand arm system: mechanical design, shape analysis and experimental validation, in: Proceedings of the IEEE/RSJ International Conference on Intelligent Robots and Systems, San Francisco-USA, 2011, pp. 1836–1842.
[34] B. Vanderborght, A. Albu-Schäeffer, A. Bicchi, E. Burdet, D. Caldwell, R. Carloni, M. Catalano, O. Eiberger, W. Friedl, G. Ganesh, M. Garabini, M. Grebenstein, G. Grioli, S. Haddadin, H. Hoppner, A. Jafari, M. Laffranchi, D. Lefeber, F. Petit, S. Stramigioli, N. Tsagarakis, M. van Damme, R. van Ham, L.C. Visser, S. Wolf, Variable impedance actuators: a review, Robot. Auton. Syst. 61 (2013) 1601–1614.
[35] R.R. Torrealba, S.B. Udelman, Design of cam shape for maximum stiffness variability on a novel compliant actuator using differential evolution, Mech. Mach. Theory 95 (2016) 114–124.
[36] A. Jafari, N.G. Tsagarakis, D.G. Caldwell, A novel intrinsically energy efficient actuator with adjustable stiffness (AwAS), IEEE/ASME Trans. Mechatron. 18 (2013) 355–365.
[37] E.C. Martinez-Villalpando, J. Weber, G. Elliott, H. Herr, Design of an agonist-antagonist active knee prosthesis, in: Proceedings of the 2nd Biennal IEEE/RAS-EMBS International Conference on Biomedical Robotics and Biomechatronics, Scottsdale-USA, 2008, pp. 529–534.
[38] S. Jezernick, G. Colombo, M. Morari, Joint-angle trajectory adaptation for the robotic orthosis Lokomat, in: Proceedings of the Workshop on European Scientific and Industrial Collaboration (WESIC), Enschede-Holland, 2001, pp. 451–456.
[39] A. Kaelin-Lang, L. Sawaki, L.G. Cohen, Role of voluntary drive in encoding an elementary motor memory, J. Neurophysiol. 93 (2005) 1099–1103.